A novel Doppler effect reduction method for wayside acoustic train bearing fault detection systems

Zhang, Dingcheng; Entezami, Mani; Stewart, Edward; Roberts, Clive; Yu, Dejie

DOI:
10.1016/j.apacoust.2018.09.017

Document Version
Peer reviewed version

Citation for published version (Harvard):
Zhang, D, Entezami, M, Stewart, E, Roberts, C & Yu, D 2019, 'A novel Doppler effect reduction method for wayside acoustic train bearing fault detection systems', *Applied Acoustics*, vol. 145, pp. 112-124. https://doi.org/10.1016/j.apacoust.2018.09.017

A Novel Doppler Effect Reduction Method for Wayside Acoustic Train Bearing Fault Detection Systems

Dingcheng zhang[1]*, Mani Entezami[1], Edward Stewart[1], Clive Roberts[1], Dejie YU[2]

1. School of Engineering, University of Birmingham, Birmingham, B152TT, United Kingdom
2. State Key Laboratory of Advanced Design and Manufacturing for Vehicle Body, Hunan University, Changsha, 410082, China

Abstract: Wayside acoustic detection of train bearing faults plays a significant role in maintaining safety in the railway transport system. Due to the relative movement between the train and the detection system, the collected acoustic signals are distorted by the Doppler Effect which results in frequency-domain distortion. Combining the multi-scale chirplet path pursuit (MSCPP) method, a variable digital filter (VDF), and a new motion parameter estimation method, a novel Doppler Effect reduction method is proposed. This can be used by wayside acoustic monitoring systems to improve detection system for train bearing faults, as illustrated in this paper. The MSCPP method with the build-in criterions is firstly used to estimate the instantaneous frequencies (IFs) of harmonic components in the wayside acoustic signals. Next, VDFs whose centre frequencies are the fitted IFs are constructed to exclude harmonic components. Using these, residual signals, free of strong harmonic interferences, can be obtained. At the same time, the motion parameters can be obtained by using a recently developed estimation method based on fitted IFs. The residual signal is then resampled to reduce the Doppler Effect by using the resampling time vector constructed using those estimated motion parameters. Finally, any bearing fault features can be extracted using the spectral kurtosis (SK) method. The effectiveness of the proposed signal processing method is verified by simulation and field-based experiments, as demonstrated in this paper.

Keywords: Doppler Effect reduction, train bearing, wayside acoustic detection, multi-scale chirplet path pursuit, variable digital filter, time-domain interpolation resampling

*Corresponding author. Tel.: +44 07422941910;
E–mail address: railcm@contacts.bham.ac.uk (Dingcheng Zhang)

1 Introduction

Train bearings are a key component of the vehicle that must support the entire weight of the train and operate at high speeds. Faults occurring in train bearings can result in economic loss or even casualties. Hence, fault detection in these key components plays a significant role in maintaining and continuing to increase role of rail in transportation networks. Wayside acoustic detection for train bearings has recently attracted increased attention because one monitoring station will observe multiple vehicles and no physical track access is required in order to install the equipment.

The signals obtained by wayside acoustic monitoring stations are distorted by the Doppler Effect due to the relative motion between the train being inspected and the detection system. The Doppler Effect results in serious frequency-domain distortion to the collected signals, which is an obstacle to train bearing fault detection. Hence, the reduction of the Doppler Effect is a key stage in wayside acoustic train bearing fault detection. The most commonly used methods of Doppler Effect reduction can be classified into two main categories: instantaneous frequency (IF)-based method, and parameter-based method.

The IF-based methods are the combination of instantaneous frequency (IF) extraction and time-domain interpolation resampling (TIR). Central to those methods are accurate IF estimation. Some methods, (e.g. Hilbert transform [1], time-frequency ridge extraction [2]) have been proposed to address this issue. In IF-based methods, the resampling time vector tr is constructed based on the IF generated by the target bearing and its invariant frequency f_o [2, 3], as shown in Eq. (1).

$$tr(k) = \sum_{i=1}^{k} \frac{f_o \cdot \Delta t_s}{f_o(t_i)} \tag{1}$$

where k is the resampling point; f_o is the stationary frequency of the signal; $f_o(t)$ is the IF curve which is the variation of f_o caused by the Doppler Effect; and Δt_s is the sampling interval for the raw signal. The advantage of this kind of method is that it is simple to implement while yet effective. However, the resonance frequency of the target bearing is difficult to estimate because of the complex structure of the rotational system. Furthermore, Eq. (1) implies two problems: (i) how to find the IFs generated by the target bearing, and (ii) how to estimate the invariant frequency f_o beforehand. Hence, these kinds of methods are rarely applied in practice.

The parameter-based method is a scheme that combines multiple motion parameters and time-domain interpolation resampling. In order to construct the resampling time vector, tr, motion parameters for the target bearing are obtained using either velocity sensor based measurements or the matching pursuit method. Using sensor based measurements, the parameters can be obtained in real time [4], but extra sensors will increase cost of the condition monitoring system. To overcome this disadvantage, researchers have proposed methods such as the Dopplerlet transform [5, 6] and the single side Laplace wavelet [7] which are based on matching a Doppler distorted correlation model to calculate the motion parameters. In these methods, the construction of tr is only based on motion parameters [8, 9], as shown in Eq. (2).

$$tr = t + \frac{\sqrt{r^2 + (s - vt)^2}}{c} \tag{2}$$

where r is the distance between the train and the microphone measured perpendicularly to the track; s is the initial distance between the train and microphone measured longitudinally along the track (as shown in Figure 4); v is the speed of the train (the speed is considered as a constant because the time for a train passing the microphone is short); t is the time within the period of detection; and c is the speed of sound. The performance of those matching pursuit methods has been verified[5-7], however constructing the matching model is a time-consuming process and thus these techniques cannot be applied in real-time condition monitoring systems.

Drawing from the strengths of both the IF and parameter based methods, researchers have proposed a novel Doppler Effect reduction method in which IF extraction and curve fitting, based on the least-squares method, are applied to estimate motion parameters [8, 10, 11]. The method has been shown to perform well, however the resonant frequencies of the target bearings can be masked by high levels of background noise such as those found in real operating conditions. Additionally, curve fitting based on the least-squares method is complex [12] and may not support real-time operation.

To overcome the above problems, a novel Doppler Effect reduction method is proposed in this paper. The method is a combination of the multi-scale chirplet path pursuit (MSCPP) method, a variable digital filter (VDF), and the new motion parameter estimation method described in [12]. The use of the MSCPP method with the build-in criteria is firstly used to extract the IFs of harmonic components found in wayside acoustic signals. The build-in criteria are used to determinate the births and

the deaths of IF curves, and the estimated IFs are then subjected to cubic-spline fitting. Secondly, the fitted curves are set as the centre frequencies of the VDFs which are constructed to exclude the main harmonic components from the collected acoustic signals. Consequently, the residual signal can be obtained. At the same time, a new method, proposed by Timlelt et al [12] and based on the obtained IFs, is used to estimate the motion parameters. These parameters are then used to construct the resampling time vector, tr, as per Eq. (2). The Doppler-free signal can be obtained by resampling the residual signal using the time-domain interpolation resampling (TIR) method. Finally, any bearing fault features can be extracted using the spectral kurtosis (SK) method. The simplified flow chart of the proposed method is shown in Figure 1.

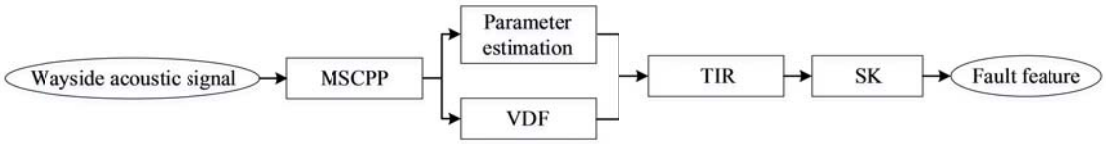

Figure 1 Simplified flow chart of the proposed method

The sections of this paper are organised as follows: In section 2, the MSCPP method is introduced. In section 3, the VDF method is introduced. Motion parameter estimation is introduced in section 4. A novel Doppler Effect reduction method based on the proposed method is presented in section 5. In section 6 and section 7, the simulation and field experiments demonstrating the proposed method are introduced. The conclusions of this paper are presented in the final section.

2 Multi-scale chirplet path pursuit

The MSCPP method was initially proposed by Candes et al. [13]. The method is based on the estimation of IFs within continuously time-varying component signals. It makes use of a multi-scale chirplet atom whose IF is a straight-line. A brief introduction to the MSCPP method is provided in the following section.

Any signal f(t) can be represented as a linear combination of a group of atoms $\{\boldsymbol{h}_n\}$, as shown in Eq. (3), where $\boldsymbol{a}_n$ is the index of the n-th atom [14]. If $\{\boldsymbol{h}_n\}$ is orthogonal, then the inner product can be used to compute $\boldsymbol{a}_n$ (Eq.(4)). Hence, $\boldsymbol{a}_n$ reflects similarity between the signal f(t) and the atom $\boldsymbol{h}_n$.

$$\mathrm{f}(t) = \sum_{n \in Z} \boldsymbol{a}_n \boldsymbol{h}_n \tag{3}$$

$$\boldsymbol{a}_n = \left\langle \mathrm{f}(t), \boldsymbol{h}_n \right\rangle / \left\| \boldsymbol{h}_n \right\| \tag{4}$$

Multi-scale chirplet atoms $\boldsymbol{h}_{a,b,\boldsymbol{I}}(t)$ are used in the MSCPP method, as follows

$$\boldsymbol{h}_{a,b,\boldsymbol{I}}(t) = \left|\boldsymbol{I}\right|^{-1/2} e^{-i(at^2/2+bt)} \mathrm{l}_{\boldsymbol{I}}(t) \tag{5}$$

where a and b are the slope and offset coefficients respectively and $at+b$ should be less than $f_s/2$ (where f_s is the sampling frequency); $\boldsymbol{I}$ is the dyadic time interval, i.e. $\boldsymbol{I} = \left[k2^{-j}, (k+1)2^{-j}\right]$ where $k = 0,1,\cdots,(2^j-1)$ and $j = 0,1,\cdots,\log_2(N-1)$, and N is the number of sampling points; $\mathrm{l}_{\boldsymbol{I}}(t)$ is the rectangular window function, which is 1 when $t \in \boldsymbol{I}$ and 0 when $t \notin \boldsymbol{I}$; and $\left|\boldsymbol{I}\right|^{-1/2}$ is the normalization factor which makes $\left\| \boldsymbol{h}_{a,b,\boldsymbol{I}}(t) \right\|_{L_2} = 1$.

Eq. (5) indicates that the IF of the multi-scale chirplet atom is $at+b$. Hence, the IF of $\mathrm{f}(t)$ can be estimated by linking the linear frequencies of the atoms together piece by piece. The optimal atom in a dyadic time interval can be obtained through calculating the maximum correlation coefficient $\boldsymbol{\beta}_{\boldsymbol{I}}$ between the atom and $\mathrm{f}(t)$ in the time interval, as shown in Eq. (6).

$$\boldsymbol{\beta}_{\boldsymbol{I}} = \max_{\boldsymbol{I}} \left\langle \mathrm{f}(t), \boldsymbol{h}_{a,b,\boldsymbol{I}} \right\rangle \tag{6}$$

where $\langle \bullet \rangle$ represents the inner product operator. In this case, $\boldsymbol{\beta}_{\boldsymbol{I}}$ contains the amplitude and the initial phase information of $\mathrm{f}(t)$ [15]. Denoting $\mathrm{c}_{\boldsymbol{I}}(t)$ as the representation of the component decomposed in the dyadic interval, this is expressed as shown in Eq. (7).

$$\mathrm{c}_{\boldsymbol{I}}(t) = \left|\beta_{\boldsymbol{I}}\right| e^{-i(at^2+bt)+\angle\boldsymbol{\beta}_I} \mathrm{l}_{\boldsymbol{I}}(t) \tag{7}$$

The best path algorithm [15] is then used to construct $\mathrm{c}_{\boldsymbol{I}}(t)$ whose time period is equal to that of signal $\mathrm{f}(t)$ and whose energy is the largest among all the possible paths, as shown in Eq. (8).

$$\max\left(\sum_{I \in \prod^n} \left\| \mathrm{c}_{\boldsymbol{I}}(t) \right\|^2\right) \quad \mathrm{s.t.}\ \prod^n = \left\{\boldsymbol{I}_1^n, \boldsymbol{I}_2^n, \cdots\right\} \in \left\{\boldsymbol{I}\right\} \tag{8}$$

where n is the number of decompositions; and $\prod^n$ represents the analysis time period without overlap. By repeating the above steps, $\mathrm{f}(t)$ can be decomposed as

$$\mathrm{f}(t) = \sum_1^n \mathrm{c}^n(t) + \boldsymbol{r}^n \tag{9}$$

where $\boldsymbol{r}^n$ is the residual signal after n-th decomposition. The energy of $\boldsymbol{r}^n$ decreases with increasing n. The decomposition is stopped if the energy of the residual signal falls below a certain threshold. Hence, for a signal with multiple components, the signal component extracted by the MSCPP method is the one with the largest energy in the signal being analysed. The instantaneous frequency of the signal component extracted by MSCPP can be estimated by concatenating the piecewise linear frequencies of the chirplets.

While this approach has been shown to work for clean signals, there are multiple IF curves and a high level of background noise in the time-frequency representations of wayside acoustic signals. In order to avoid crossover between IFs, and to find the true IF curves of the harmonic components, the use of an energy contribution coefficient $\theta_i (i = 1,2,\cdots,N)$ is proposed, as shown in Eq. (10).

$$\theta_i = \frac{\mathrm{E}(\mathrm{TFR}(\mathrm{IF}_{j=1,2,\cdots,\mathrm{N},j\neq i}))}{\mathrm{E}(\mathrm{TFR}(\mathrm{IF}_{1,2,\cdots,\mathrm{N}}))} \tag{10}$$

where $\mathrm{IF}_{1,2,\cdots,N}$ is the instantaneous frequency vector. $\mathrm{IF}_{j=1,2,\cdots,N,j\neq i}$ is the instantaneous frequency vector without the i-th point; $\mathrm{TFR}(\bullet)$ is the amplitude of the time-frequency representation obtained using a short-time Fourier transform; $\mathrm{E}(\bullet)$ represents the energy of the vector. θ_i has a greater value if the i-th point has a lesser contribution to the energy of the IF component, and vice-versa. The energy contribution coefficient vector $\theta = (\theta_1, \theta_2, \cdots, \theta_N)$ is normalised as $\hat{\theta}$, as shown in Eq. (11)

$$\hat{\boldsymbol{\theta}} = \frac{\boldsymbol{\theta} - \boldsymbol{\theta}_{\min}}{\boldsymbol{\theta}_{\max} - \boldsymbol{\theta}_{\min}} \tag{11}$$

where and $\boldsymbol{\theta}_{\max}$ and $\boldsymbol{\theta}_{\min}$ are the maximum and minimum values of $\boldsymbol{\theta}$ respectively.

Two build-in criteria for the MSCPP method are proposed to determine the births and the deaths of the IF curves caused by the Doppler Effect, as shown as Eq. (12).

$$\begin{cases} \mathrm{TFR}(\mathbf{IF}_{i,j}) \geq \hat{\boldsymbol{\theta}}\,\mathrm{M}(\left|\mathrm{TFR}(\mathbf{IF}_i)\right|) \\ \mathbf{IF}_{i,\mathbf{I}_{k+1}(\mathrm{start})} - \mathbf{IF}_{i,\mathbf{I}_k(\mathrm{end})} < 0 \end{cases} \tag{12}$$

where $\mathbf{IF}_{i,j}$ is the j-th point in the i-th IF curve; $\mathbf{IF}_{i,\mathbf{I}_{k+1}(\mathrm{start})}$ and $\mathbf{IF}_{i,\mathbf{I}_k(\mathrm{end})}$ are the start point of the (k+1)-th time interval and the end point of the k-th time interval in the i-th IF curve, respectively; $\mathrm{M}(\left|\bullet\right|)$ represents the mean operation of the absolute value.

The sections of IF curves with minor amplitude values are easily influenced by background noise and other components in the time-frequency domain, which easily results in relatively large errors for motion parameter estimation. Hence, the first criterion in Eq. (12)is proposed to exclude IF sections with minor amplitude values in the time-frequency domain. In addition, the IF curves caused by the Doppler Effect monotonically decreases according to Eq. (17). What's more, the background noise will influence the slope of the IF sections in some time intervals $\boldsymbol{I}$ in real operating conditions. Hence, the second criterion in Eq. (12), as a compromise, is proposed. Through considering both criterions in Eq. (12), the births and deaths of interested IF sections can be identified.

3 Variable digital filter with zero-phase shift

A variable digital filter is constructed and used to exclude harmonic components from the collected wayside acoustic signal. The fitting line of the IF obtained using the MSCPP method is used as the centre frequency of the VDF.

The transform function of the VDF $\mathrm{H}(s,t)$ can be obtained by changing the frequency variable s' in that of original filter $\mathrm{H}(s')$ [16], that is $\mathrm{H}(s,t)=\mathrm{H}(s')$. The Chebyshev □ filter is selected as the base filter used in this paper. The main reasons for this are that its amplitude response function is steep in the transition band and decreases monotonously. As described in [16], the relationship between s and s' is

$$\begin{cases} s'=\dfrac{s\omega_c}{\left[\omega_z(t)+b_w(t)/2\right]} \\ \quad \omega_z(t)-b_w(t)/2\le 0 \\ s'=\dfrac{\omega_c\left\{s^2+\left[\omega_z(t)-b_w(t)/2\right]\left[\omega_z(t)+b_w(t)/2\right]\right\}}{sb_w(t)} \\ \quad \omega_z(t)-b_w(t)/2>0\ \&\ \omega_z(t)+b_w(t)/2<\omega_s/2 \\ s'=\dfrac{\omega_c\left[\omega_z(t)-b_w(t)/2\right]}{s} \\ \quad \omega_z(t)+b_w(t)/2<\omega_s/2 \end{cases} \tag{13}$$

where ω_c is the cut-off frequency of the classical low-pass filter $\mathrm{H}(s')$; ω_s is the sampling frequency; and ω_z and b_w are the centre frequency and bandwidth of the VDF, respectively.

By design, the centre frequency for the VDF changes with time. This may result in phase shift and hence signal distortion. Hence, a forward-backward filter is used to eliminate phase shift. The forward-backward filter algorithm is a common tool used to create a zero-phase nonlinear filter [17, 18]. Examples of the use of a forward-backward filter to obtain a phase shift-free signal can be found in [18-20].

The Empirical Mode Decomposition (EMD) method is one of the most commonly used methods for nonlinearly separating components of a signal [21]. To verify the effectiveness of the MSCPP and the VDF method, a comparison with respect to the EMD method is conducted; results are shown in Figure 2. Three simulated test signals with different SNR but all including the same two harmonic components influenced by the Doppler Effect are used in the comparison. Their time domain waveforms are shown in Figure 2 (a). Both harmonic components are constructed according to acoustic theory as described in [22]. The motion parameters are set as: $v = 35$ m/s, $c = 340$ m/s, $r = 0.2$ m, $fs = 8192$ Hz. In addition, the initial longitudinal distance (along the track) and stationary frequency for both components are ($s_1 = 2$ m, $f_1 = 200$ Hz) and ($s_2 = 4$ m, $f_2 = 100$ Hz) respectively. The signal-to-noise ratios (SNR) for the three simulated signals are different, i.e. noise does not exist in the first signal and the SNR for the latter two signals are 0 dB and -5 dB respectively. Figure 2 (b) and (c) shows the results after the simulated signals are subjected to the MSCPP+VDF and EMD methods respectively. Figure 2 (b) shows that the MSCPP+VDF method can be used to extract the elements of harmonic components with high energies effectively. Intrinsic mode functions (IMFs) corresponding to two harmonic components are obtained by using the EMD method [23], which are shown in Figure 2 (c). Figure 2 (c) shows that the EMD method has limited capacity for the separation of harmonic components influenced by Doppler Effect. It can be seen from Figure 2 that the MSCPP+VDF method has a greater capability for resisting noise than the EMD method. Hence, the MSCPP+VDF method is considered to be advantageous in the separation of multiple harmonic components influenced by the Doppler Effect.

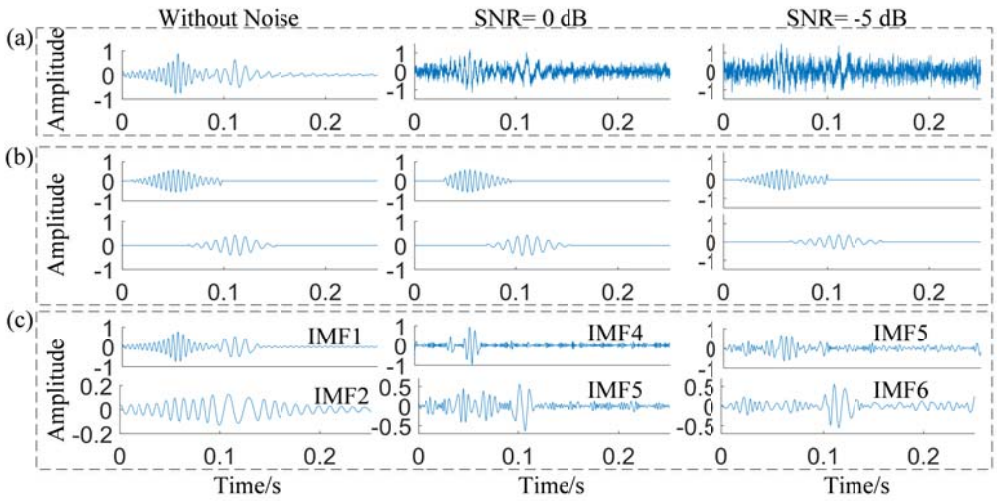

Figure 2 Comparison experiment (a) Time domain waveform for simulated signals with different SNR (b) Results after using the MSCPP+VDF method (c) Intrinsic Mode Functions (IMFs) after using the EMD method

4 Motion parameter estimation for train bearings

The basic layout of the wayside acoustic detection system discussed in this paper is shown in Figure 3. The system includes a microphone, a pair of light-gates, a sonic anemometer and recording equipment. The light-gates are used to trigger the recording system and thus the time when the target bearing passes the microphone, tc, can be identified and used to specify the detection period (range of t) for the target bearing passage. With the perpendicular distance between the train (r) and the speed of sound (c) directly measureable, only v and s need to be estimated in order to construct the resampling time vector tr as per Eq. (2). This can then be used to reduce the Doppler Effect in the recorded signals.

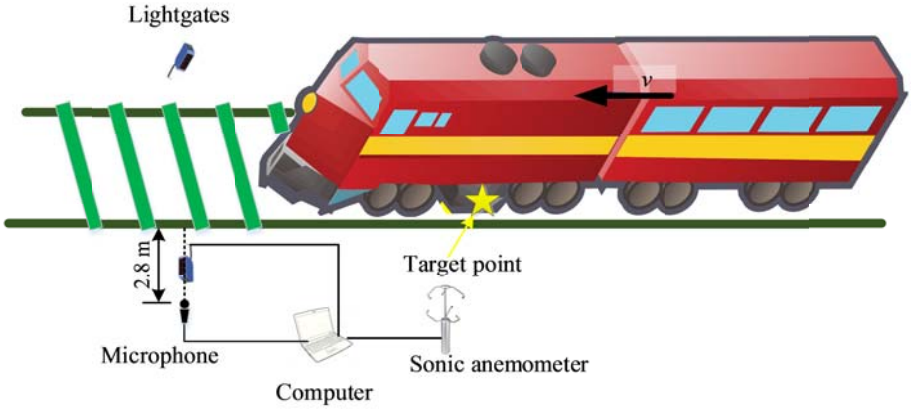

Figure 3 Basic layout of the wayside acoustic detection system

Motion parameter estimation for a moving source is a current topic of interest. Recently, a new estimation method based on IF extraction proposed by Timlelt et al.

is a closed-form solution which is less complex and thus suitable for hardware implementation [12]. In this paper, the method is used to estimate the motion parameters of train bearings.

Figure 4 shows a schematic diagram of a wayside acoustic detection system for train bearings. An acoustic signal emitted by a sound source in the train (not necessarily a bearing) at time τ is received by the microphone at time t. The distance between the sound source and the microphone, d, varies with time. t_c is the time when the sound source passes the closest point of approach (CPA), i.e. when the sound source passes directly in front of the microphone. This corresponds to d being equal to r and s being zero.

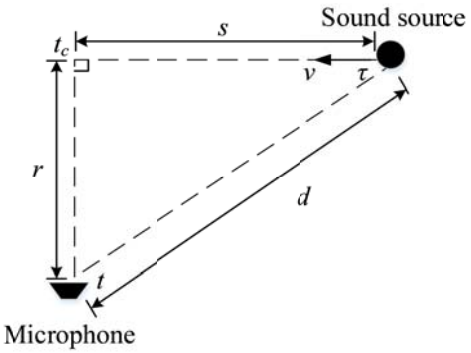

Figure 4 Schematic diagram of a wayside acoustic detection system for train bearings

Assuming a received acoustic signal x(t) generated by i $(i = 1, \cdots, n)$ sound sources is as shown as in

$$\mathrm{x}(t) = \sum_{i=1}^{n} \mathrm{A}_i(t)\cos[\theta_i(t)] \tag{14}$$

where $\mathrm{A}_i(t)$ and $\theta_i(t)$ are the amplitude variation and the phase variation of the i-th sound source with the Doppler Effect. The distance d and the time τ are given by Eq. 15 and Eq. 16, respectively [12].

$$d = (t - \tau)c = \sqrt{r^2 + v^2(\tau - t_c)^2} \tag{15}$$

$$\tau = \frac{c^2 t - v^2 t_c - \sqrt{r^2(c^2 - v^2) + v^2 c^2 (t - t_c)^2}}{c^2 - v^2} \tag{16}$$

The i-th IF of the received signal $\mathrm{f}_i(t)$ at time t can be represented as Eq. 17, because $\theta_i(t)$ is equal to $2\pi f_o \tau$. Then substituting Eq. 16 in Eq. 17, Eq. 18 can be obtained as below.

$$\mathrm{f}_i(t) = \frac{1}{2\pi}\frac{\mathrm{d}\theta_i(t)}{\mathrm{d}t} = f_o\frac{\mathrm{d}\tau}{\mathrm{d}t} \tag{17}$$

$$\mathrm{f}_i(t) = \frac{f_o c^2}{c^2 - v^2}\left(1 - \frac{v^2(t - t_c)}{\sqrt{r^2(c^2 - v^2) + v^2c^2(t - t_c)^2}}\right) \tag{18}$$

where f_o is the constant frequency of the i-th acoustic tone. c is the speed of sound in the air. In general, c can be calculated using the temperature and humidity as over this scale it is not heavily influenced by the wind. Or, as in the field experiments carried out here, it can be measured. In this case an R3-50 sonic anemometer was used to measure the speed of sound [4]. The derivative of Eq. (18) gives:

$$\mathrm{f}_i{}'(t) = \frac{v^2r^2(c^2 - v^2)\mathrm{f}_i(t_{ci})}{\sqrt{[r^2(c^2 - v^2) + v^2c^2(t^2 - {t_{ci}}^2)]^3}} \tag{19}$$

It can be seen from Eq. (19) that $\mathrm{f}_i{}'(t)$ is less than zero, that is, $\mathrm{f}_i(t)$ in Eq. (18) has a monotonically decreasing trend. To determine an estimation of the CPA time (te_{ci}) for the i-th sound source, the maximum value of the IF derivative is used, as shown in Eq. (20).

$$te_{ci} = \mathrm{Arg\,max}\left|\mathrm{f}_i{}'(t)\right| \tag{20}$$

The estimation of train speed, ve_i, is shown as follows:

$$ve_i = \sqrt{\frac{\sum_{t=1;t\neq te_{ci}}^{N} c^2[(t - te_{ci})\mathrm{f}_i{}'(te_{ci})]^2[\mathrm{f}_i(te_{ci}) - \mathrm{f}_i(t)]^2}{\sum_{t=1;t\neq te_{ci}}^{N}([(t - te_{ci})\mathrm{f}_i{}'(te_{ci})]^2 - [\mathrm{f}_i(te_{ci}) - \mathrm{f}_i(t)]^2)\mathrm{f}_i(te_{ci})^2}} \tag{21}$$

where te_{ci} is the estimated value of t_c for the i-th sound source. There is a minor error between the true and estimated IFs associated with each sound source. These errors are not systematic, and hence an average of the estimated values from a number of sound sources should be used to provide an accurate estimate of train speed, vea. The process for estimating the train speed is summarised in Figure 5.

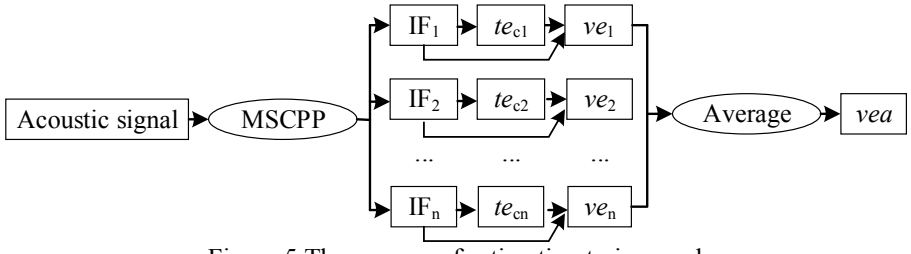

Figure 5 The process of estimating train speed

The estimated initial longitudinal distance between where the target bearing enters the detection region and the microphone (along the track), se, is

$$se = vea(t_{ct} - t_0) \tag{22}$$

where t_0 is the time when the target bearing enters the detection zone and t_{ct} is the CPA time for the target bearing. Eq. (21) and Eq. (22) show that motion parameters (v, s) can be estimated after extracting the IFs of harmonic components of the recorded acoustic signals. By substituting (vea, se) into Eq. (2), the resampling time vector tr can be obtained. Hence, the Doppler-free signal can be constructed by using the TIR method.

5 A novel Doppler Effect reduction method for wayside acoustic detection of train bearing faults

In this paper, a novel method combining the multi-scale chirplet path pursuit (MSCPP) method, a variable digital filter (VDF) and a new motion parameter estimation method is proposed to remove the Doppler Effect from wayside acoustic signal associated with train axle bearings. In the proposed method, IFs of the harmonic components are first extracted using the multi-scale chirplet path pursuit (MSCPP) method. A cubic-spline is then used to fit standard curves to the extracted IFs. Next, the motion parameters (v, s) associated with the curves are estimated using the new motion parameter estimation method. At the same time, the curves are used to define the centre frequencies of a series of VDFs. In this work, the VDF bandwidth is set to be 15 Hz. The VDFs are then used to exclude the unwanted harmonic components of the signal which are assumed to be noise. In this work, the process is repeated until the duration of the shortest IF is less than 0.25 of the detection period (i.e. one sixteenth of a second). The motion parameters can be obtained through an average of multiple harmonic components, and from these the resampling time vector can also be calculated. At the same time, a residual signal can be obtained by using the VDFs to exclude strong harmonic components. From these two things, the Doppler-free signal can be obtained by subjecting the residual signals to the time-domain interpolation resampling (TIR) method. Finally, the fault feature signal can be extracted from the Doppler-free signal using the spectral kurtosis method. Bearing faults can thus be detected by observing the Hilbert envelope of the fault feature signal. A flow chart describing this method is shown in Figure 6.

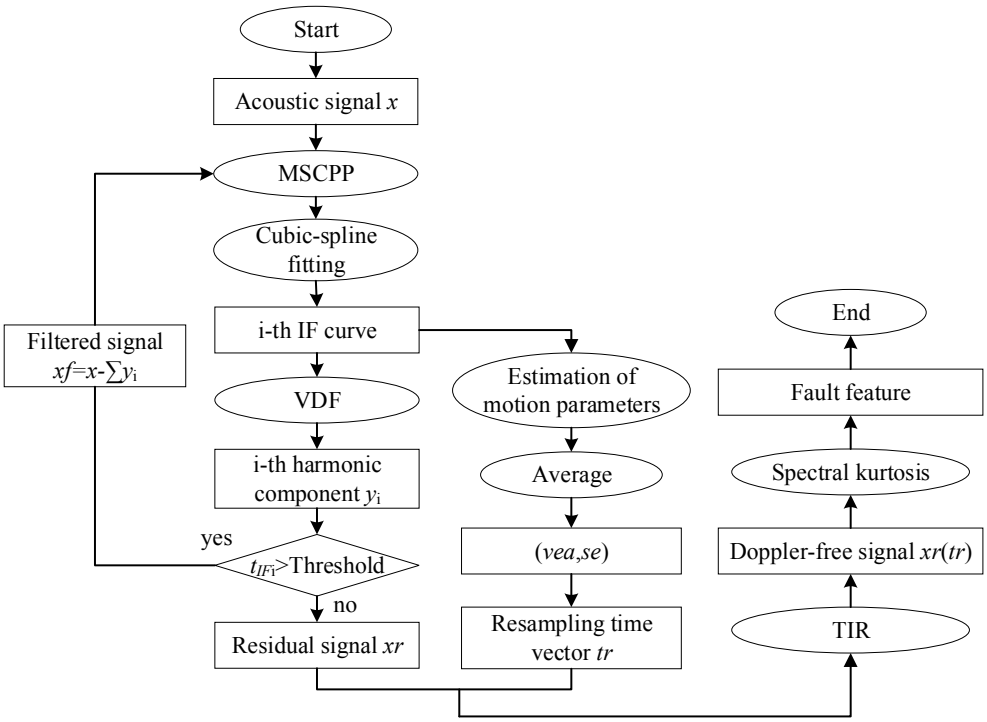

Figure 6: Flow chart for the proposed method

6 Verification by simulation

Based on acoustic theory described by Morse [22], the collected sound pressure at the microphone P can be expressed as Eq. (23) when the sound source is given as harmonic with an intensity of $q = q_0 \sin(\omega_0 t)$.

$$P = \frac{q_0 \omega_0}{4\pi d(1 - M\cos\theta)} \times \cos(\omega_0 (t - d/c)) \tag{23}$$

In Eq. (21), d is the distance between the sound source and the microphone; and $M = v/c$ (v is the train speed and c is the speed of sound). As previously discussed, the variation of the frequency is described by Eq. (16).

To verify the effectiveness of the proposed method, a simulated signal is constructed according to the standard practices as described in [10, 24]. The simulated signal is shown in Eq. (22). In practice, there are many components in a collected acoustic signal including those with strong harmonic elements. Thus, 6 harmonic components $h_{i=1\ldots5}$ and a Gaussian noise $n(t)$ are added to a weak periodical impulse signal $s(t)$ to simulate a bearing fault signal whose signal-to-noise rate is -5dB. In the simulated signal, the fault feature frequency, f_c, is set to 160 Hz. The resulting simulated signal represents a wayside acoustic signal of a train bearing, including the Doppler Effect, reconstructed according to Morse's acoustic theory as described in

[22]. The motion parameters of sound sources for the harmonic components and the impulse signal are given in Table 1. The sampling frequency is 8192 Hz and the sampling time is 0.25 s. The train speed, v, and speed of sound, c, are set to 35 m/s and 340 m/s, respectively. The amplitude values, A, of each component are shown in Table 1.

$$x(t) = s(t) + \sum_{i=1}^{6} h_i(t) + n(t) \tag{24}$$

Table 1 Motion parameters of the harmonic components and the impulse signal

	h_1	h_2	h_3	h_4	h_5	h_6	s
s	2	2	2	4	4	4	4
r	0.5	0.8	1.2	0.5	0.5	0.8	0.5
A	1.5	1	1	1.5	1.8	1	0.5
t_c	0.057	0.057	0.114	0.114	0.114	0.114	0.114
f_o	250	150	200	100	45	75	1500

The simulated signal, which includes Doppler Effect components, is shown in Figure 7 (a). Its Hilbert envelope spectrum and time-frequency representations (TFR) are shown in Figure 7 (b) and (c). These indicate that the fault information is masked by strong harmonic components and background noise.

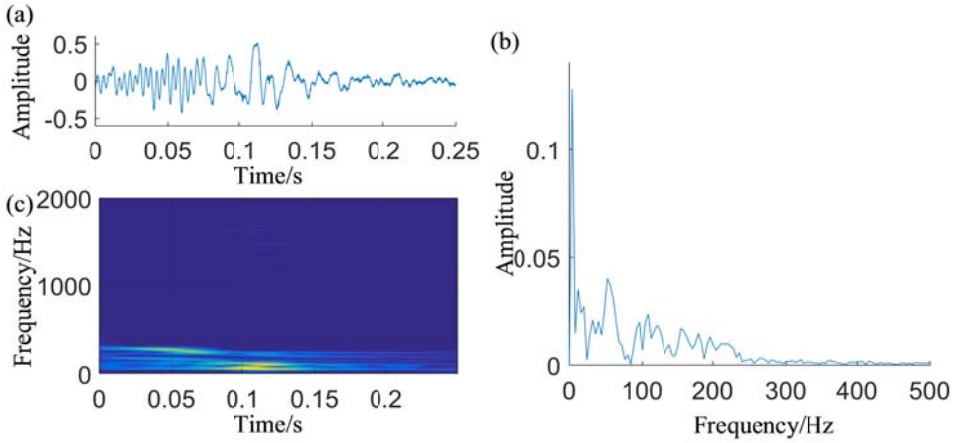

Figure 7 Simulated signal. (a) time domain waveform (b) Hilbert envelope spectrum (c) time-frequency representation of the simulation signal

The MSCPP method is used to extract IFs of the harmonic components in the simulated signal with Doppler Effect. The extracted IFs are shown in Figure 8. The dashed black lines in the figure represent the IFs of the harmonic components. The solid blue lines represent cubic-spline fittings associated with each IF curve. The fitting lines are used to estimate the velocity values as shown in Table 2. Hence, the

train speed can be estimated to be 35.66 m/s. Given a known t_c in the simulated signal (t_c=0.116), the estimate for the initial longitudinal distance between the train and the microphone (along the track) would therefore be 4.14 m, as per Eq. 22. Substituting these parameters (vea, se) into Eq. (2), the resampling time vector, tr, can be obtained as shown in Figure 9.

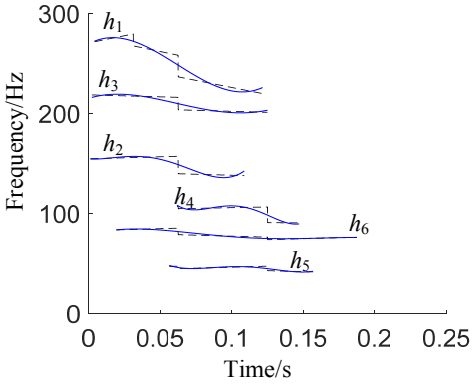

Figure 8 IFs extracted by MSCPP and fitting curves

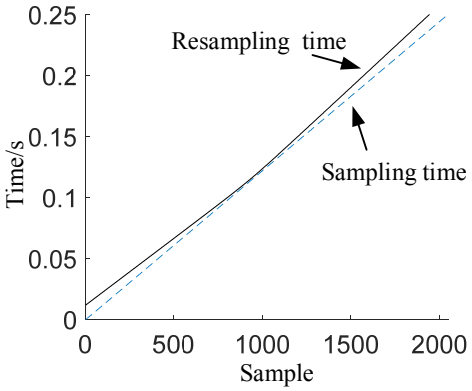

Figure 9 Time vectors

Table 2 Estimated velocity values for harmonic components

	h_1	h_2	h_3	h_4	h_5	h_6
ve	43.4	31.94	33.28	34.46	34.06	36.82

A series of variable digital filters whose centre frequencies are based on the fitted values of the IF curves are constructed in order to exclude harmonic components which would otherwise dominate the fault signals. The residual signal can then be resampled according to the resampling time vector, tr. The time domain waveform of the resampled signal is shown in Figure 10(a). Figure 10 (b) and (c) show the Hilbert envelope spectrum and TFR of the resampled signal respectively. Comparing Figure 7(c) and Figure 10(c), it can be seen that the main harmonic components are excluded, and that the residual harmonic components still exist. Figure 10 (b) shows that there is no obvious peak at f_c or any of its harmonics, which results in misdiagnosis.

The resampled signal is subjected to the SK method with the result shown in Figure 11. Figure 11 (a) shows the time domain waveform of the fault feature signal. Comparing this with Figure 10 (a), the impulse signal is more clearly evident and the residual harmonic components are excluded. This is confirmed by the TFR of the fault feature signal as shown in Figure 11 (c). Peaks at f_c, $2f_c$ and $3f_c$ are prominent in

the Hilbert envelope spectrum of the fault feature signal shown in Figure 11 (b). Hence, the effectiveness of the proposed method is demonstrated.

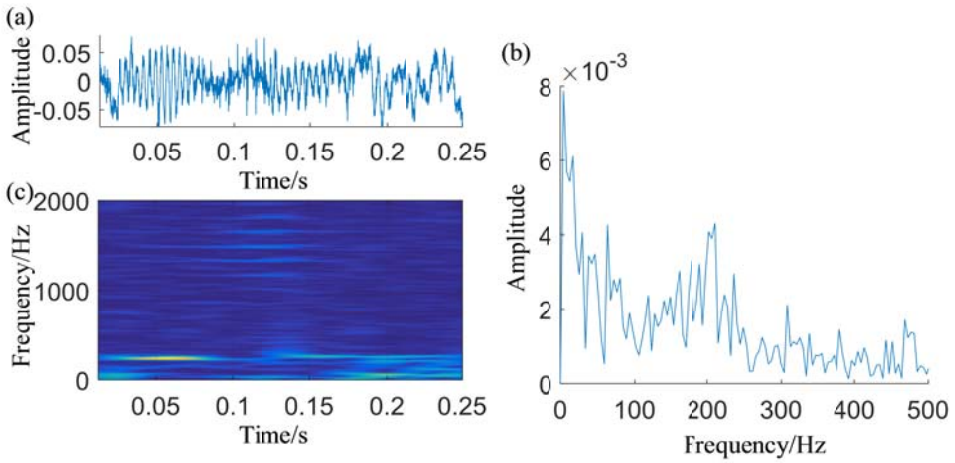

Figure 10 the resampled signal without Doppler Effect (a) time domain waveform (b) Hilbert envelope spectrum (c) time-frequency representation of the resampled signal.

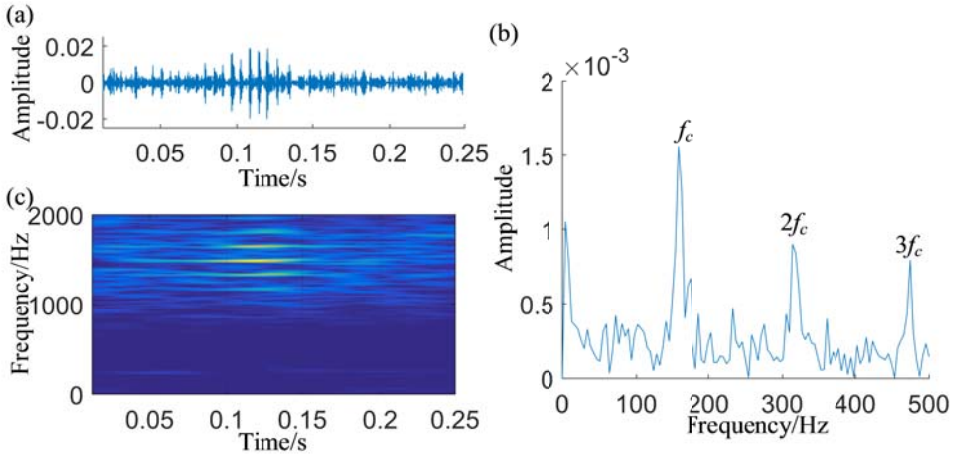

Figure 11 Fault feature signal extracted by SK (a) time domain waveform (b) Hilbert envelope spectrum (c) time-frequency representation of the fault feature signal

To test the anti-noise ability of the proposed method, several simulation signals with different SNR values are constructed. The estimated values of *vea* and the relative errors ε ($\varepsilon = |vea - v|/v$) can be obtained by using the proposed method, as shown in

Table **3**. The table shows that the ε will increase with SNR. Figure 12 demonstrates that Hilbert envelope spectra of fault feature signals which are extracted from the simulation signals with different SNR using the proposed method. When the SNR is equal to -9 dB, the fault feature frequency, f_c, or its harmonics is hard to be found in Figure 12 (d).

Table 3 The values of *vea* and ε for simulation signals with different SNR

SNR	-6	-7	-8	-9
vea	35.72	36.27	37.13	39.54
ε	2.1%	3.6%	6.1%	13%

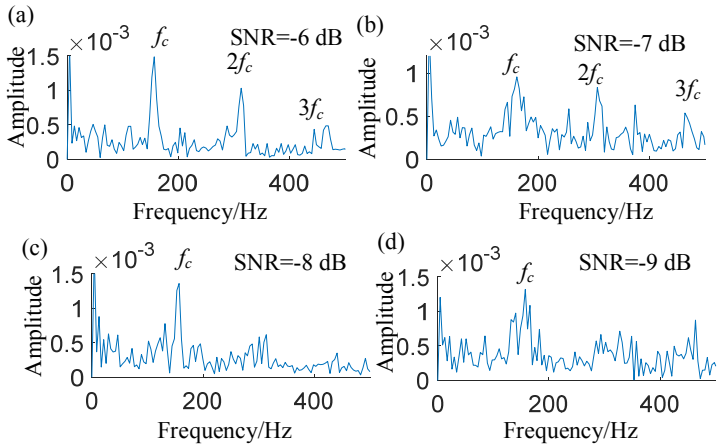

Figure 12 The Hilbert envelope spectra of the fault feature signals extracted from simulation signals with different SNR.

7 Verification using field experiments

In order to test the performance of the proposed method in a real railway environment, acoustic signals were collected from the wayside as a test train was passing. The wayside acoustic system is represented in Figure 3 and described in [4] although in this experiment data from only one microphone within the array system was considered. The test train consisted of a single car of a DMU hauling two test wagons, as shown in Figure 13 (a). The speed of the test train through the monitored section was approximately 13.5 m/s, i.e. approximately 278 RPM for a wheel size of 0.9 m. For safety reasons, it was not possible to operate a train with known faulty bearings, so instead a loudspeaker was fitted to the third axle of the train and an acoustic signal recorded from bearings being operated in the test facility was played in order to simulate a vehicle with a bearing fault. Ground reflections were reduced both by selection of a test site with an open and grassed area to disperse reflections, and the use of an acoustic barrier as part of the construction of a wedge shaped acoustic funnel, again described in [4]. Two cases were considered, Case 1 represents a fault in the outer race, while Case 2 represents a roller fault. These are shown as Figure 13 (b) and (c). In order to align the recordings with the speed of the train, the rotational speed used during the laboratory measurements was approximately 270 RPM. The sampling frequency used was 8192 Hz. The parameters of the test

bearing are shown in . The roller passing frequency outer race f_{RPFO} and the roller fault frequency f_{RFF} are approximately 43Hz and 35Hz as calculated using Eq. (23) and Eq. (24), respectively.

Table 4 Test bearing parameters

Type	Number of rollers n	Roller diameter RD	Pitch diameter PD	Contact angle β
TAROL 130/230-U-TVP	22	24 mm	187 mm	6.9°

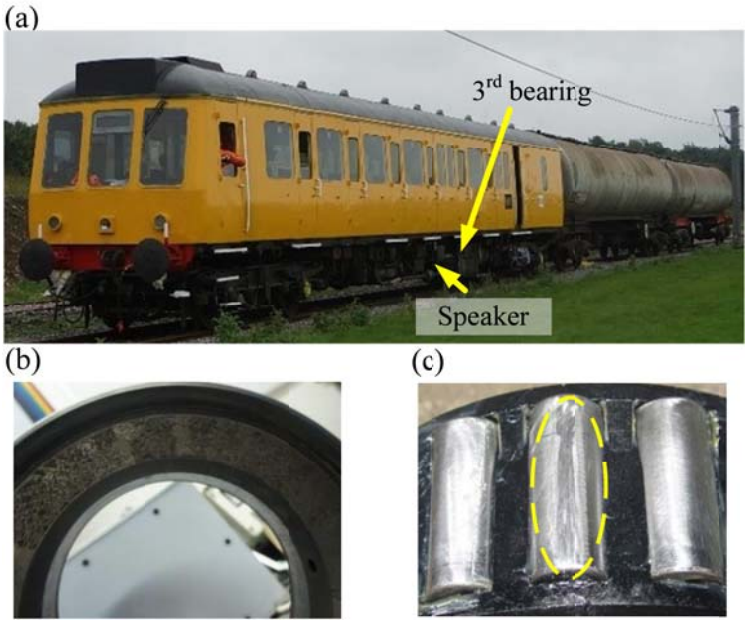

Figure 13 (a) Test train (b) Test bearing with outer race fault (c) Test bearing with roller fault

$$f_{RPFO} = \frac{n}{2}\left(1 - \frac{RD}{PD}\cos\beta\right) f_r \tag{25}$$

$$f_{RFF} = \frac{PD}{RD}\left(1 - \left(\frac{RD}{PD}\cos\beta\right)^2\right) f_r \tag{26}$$

Case 1: Outer race fault detection

The time domain waveform of the field test signal corresponding to the outer race fault is shown as Figure 14 (a); the black line corresponds to the signal from the light-gate aligned with the microphone. Figure 14 (b) shows the section of the signal selected for analysis, which is taken when the 3rd bearing passes the microphone, tc =5.617 s. The signal section is divided into two parts, i.e. L1 and L2, by the light-gate signal as shown in Figure 14 (b). L1 corresponds to an 800 sample section before the

bearing passes the light gate (and microphone), and L2 a 1248 sample section after. The detection period is the range of time associated with the passage of the bearing past the microphone and between L1 and L2. It is chosen based on vehicle speed, wheel diameter, and bearing geometry to ensure that all elements of the bearing are observed while being loaded. In this work, the detection period is selected to be 0.25 s as the wheel diameter is 0.9 m and the vehicle assumed to have a minimum speed of 40 Km/h.

The TFR and the Hilbert envelope spectrum of the signal being analysed are shown in Figure 14 (c) and (d) respectively. Figure 14 (d) shows that the fault information is masked by strong harmonic interference (at 20 Hz) and background noise, which result in miss-diagnosis.

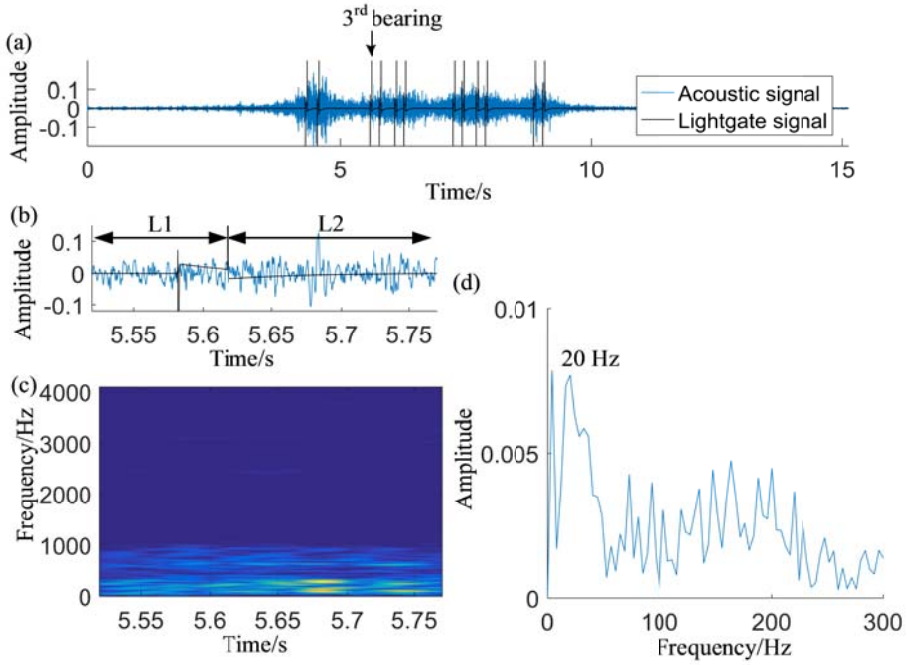

Figure 14 Acoustic signal collected by wayside acoustic detection system - Case 1 (a) the time domain waveform of the collected signal (b) the time domain waveform of the section signal selected for analysis signal (c) TFR of the analysis signal (d) Hilbert envelope spectrum of the analysis section

The signal section to be analysed is subjected to the MSCPP method and the extracted IF curves corresponding to harmonic components are shown in Figure 15. The dashed black lines in Figure 15 are IF curves. Curve fitting is used to estimate the motion parameters. The fitted curves are shown as solid blue lines in Figure 15, and the velocity values are given in Table 5. Thus, the train speed, vea, is found to be 13.34 m/s using Eq. (21) and the initial longitudinal distance between the train and the microphone, se, can be found to be 1.34 m. In Table 5, the relative error, ε, between

the estimated speed, *vea*, and the actual speed, *v*, shows that the proposed method can be used to estimate the actual speed accurately. In addition, the highest-energy IF ridge extracted in TFR plane using the STFT method is applied to the motion parameter estimation, comparing with the MSCPP method. The estimated motion parameters using the STFT method is shown in Table 5 which demonstrates that the MSCPP method has an obvious advantage.

Table 5 Estimation motion parameter values of for harmonic components - Case 1

	ve (h_1)	*ve* (h_2)	*ve* (h_3)	*vea*	ε	*se*
MSCPP	15.98 m/s	14.47 m/s	9.56 m/s	13.34 m/s	1.2%	1.34 m
STFT	14.76 m/s	16.34 m/s	12.35 m/s	14.48 m/s	7.3%	1.45 m

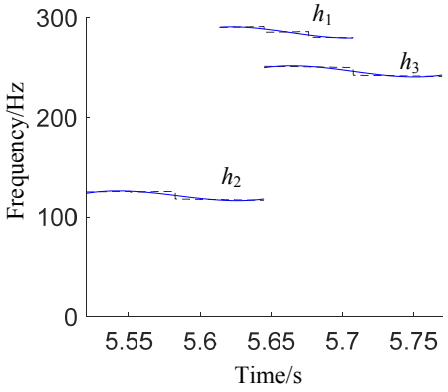

Figure 15 IFs of harmonic components for field test Case 1

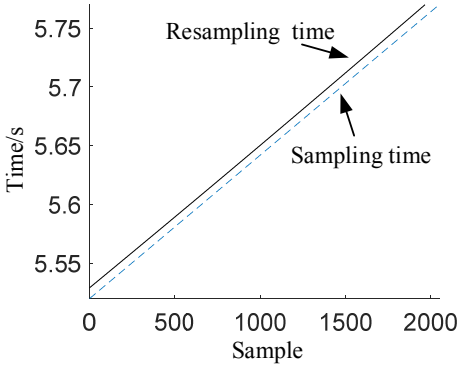

Figure 16 Time vectors in Case 1

Substituting these parameters (vea, se) into Eq. (2), the resampling time vector tr can be obtained, as shown in Figure 16 .Variable digital filters are then constructed to exclude the harmonic components whose centre frequencies are obtained by fitting curves to the IF curves obtained using the MSCPP method. The residual signal can be obtained and resampled according to the resampling time vector, tr . The time domain waveform of the resampled signal is shown in Figure 17 (a). Comparing this with Figure 19 (b), the harmonic components have been removed. This can be verified by observing the TFR of the resampled signal, as shown in Figure 17 (c). The Hilbert envelope spectrum of the resampled signal as shown in Figure 17 (b) indicates that the bearing fault feature is still masked by high levels of background noise and residual harmonic components, most notably at 12.5 Hz and 141.7 Hz. In order to overcome this, the resampled signal is next subjected to the spectral kurtosis method. The time domain waveform of the extracted fault feature signal is shown in Figure 18 (a). The Hilbert envelope spectrum and TFR of the fault feature signal are shown in Figure 18

(b) and (c) respectively. Figure 18 (b) shows peaks at f_{RPFO} and $3f_{RPFO}$, which indicates the presence of an outer race defect in the test bearing.

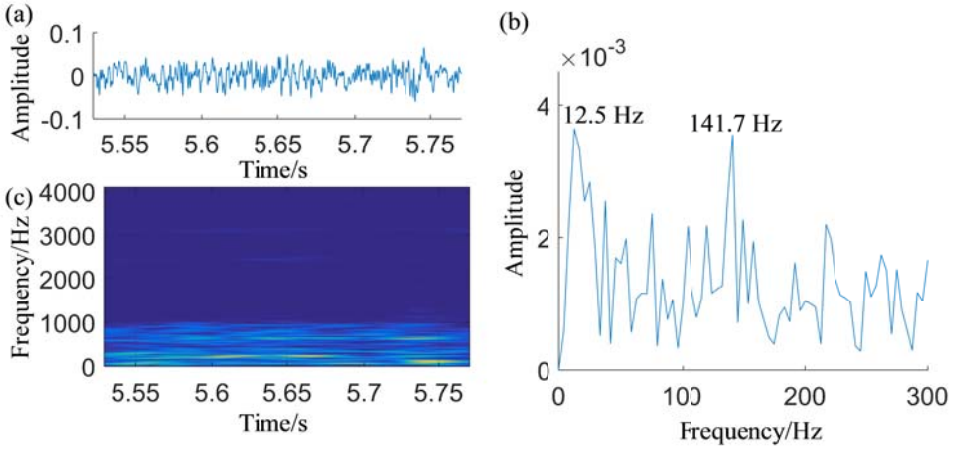

Figure 17 The resampled signal without Doppler Effect in case 1 (a) time domain waveform (b) Hilbert envelope spectrum (c) time-frequency representation of the resampled signal

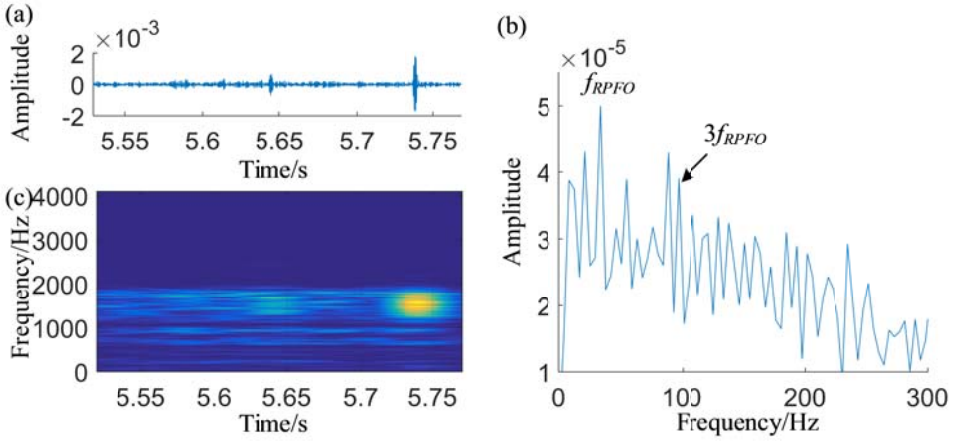

Figure 18 Fault feature signal extracted by SK - Case 1 (a) time domain waveform (b) Hilbert envelope spectrum (c) time-frequency representation of the fault feature signal

Case 2: Roller fault detection

Figure 19 (a) shows the time domain waveform of the acoustic signal with the roller fault recorded during the field tests; the black line corresponds to the signal from the light-gate aligned with the microphone. This corresponds to the time when the 3rd bearing passes the microphone, tc=5.394 s. A section of the collected signal with 2048 sampling points, as shown in Figure 19 (b), is selected for analysis based on the position of tc. As with Case 1, the section of the analysis signal is divided into two parts L1 and L2 whose length are 800 points and 1248 points respectively. The TFR and the Hilbert envelope spectrum of the section signal are shown in Figure 19 (c) and (d) respectively. These indicate that the fault feature signal is masked by

strong harmonic components (e.g. at 31Hz) and background noise, which results in miss-diagnosis.

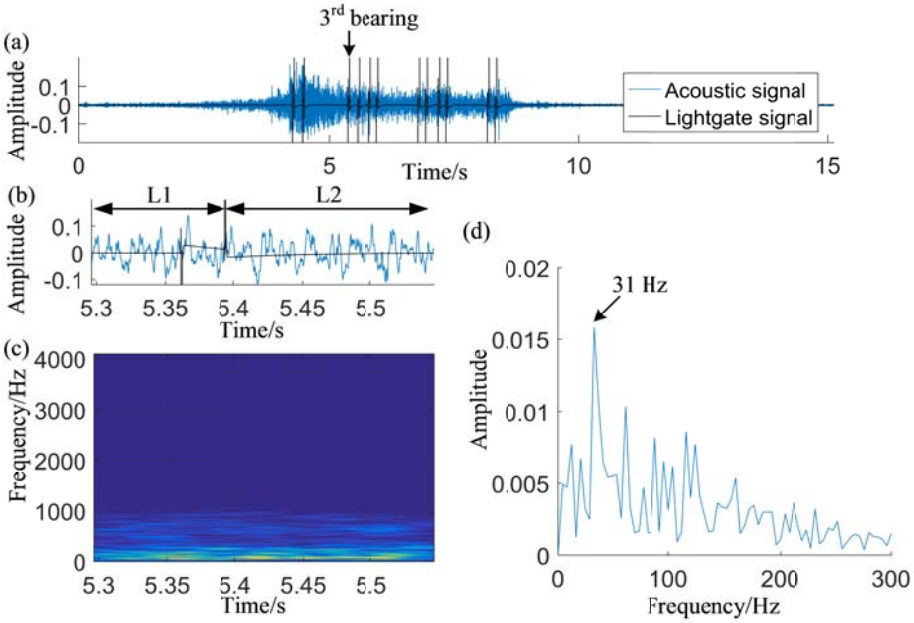

Figure 19 Acoustic signal collected by wayside acoustic detection system - Case 2 (a) the time domain waveform of the collected signal (b) the time domain waveform of the section signal selected for analysis (c) TFR of the analysis section (d) Hilbert envelope spectrum of the analysis signal

Figure 20 shows the result of applying the MSCPP method to the fault signal section. Five curves, corresponding to harmonic components, are extracted and curves are fitted to them. As with Case 1, the fitted curves are used to estimate the velocity values which are given in Table 6. Thus, the estimated train speed , vea , is found to be 14.04 m/s and the initial longitudinal distance between the train and microphone, se , is 1.37 m, as described by Eq. (22). Also, the estimated motion parameters by using the STFT method are shown in Table 6, which demonstrates the superiority of the MSCPP method. Then, Substituting these parameters (vea, se) into Eq. (2), the resampling time vector, tr , can be obtained, as shown in Figure **21**.

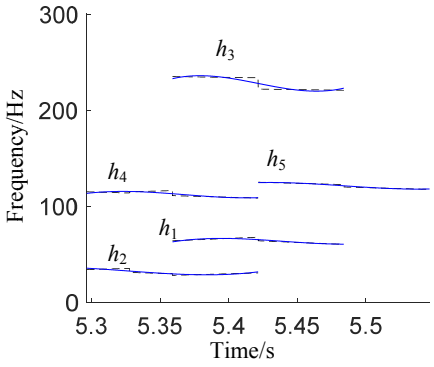

Figure 20 IFs of harmonic components for field test Case 2

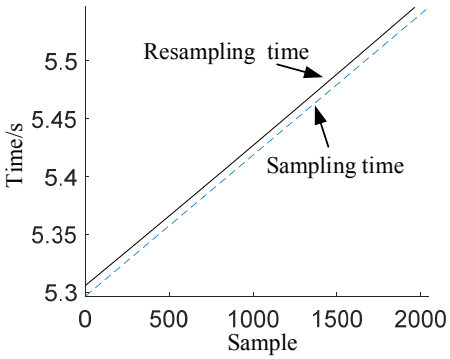

Figure 21 Time vectors in Case 2

Table 6 Estimated motion parameter values for harmonic components - Case 2

	ve (h_1)	*ve* (h_2)	*ve* (h_3)	*ve* (h_4)	*ve* (h_5)	*vea*	*ε*	*se*
MSCPP	22.77 m/s	10.78 m/s	12.88 m/s	10.7 m/s	13.07 m/s	14.04 m/s	4%	1.37 m
STFT	23.12 m/s	11.31 m/s	13.56 m/s	12.05 m/s	14.67 m/s	14.94 m/s	10.7%	1.46 m

As with the first field test case, variable digital filters are constructed using centre frequencies based on the fitted curves. The residual signal obtained after the main harmonic components are excluded using the VDFs is then resampled according to tr and thus a signal free of the Doppler Effect can be obtained. The SK method is used to extract fault feature signals from the Doppler-free signal and the result is shown in Figure **22**. Figure **22** (b) (the Hilbert envelope spectrum) shows peaks at f_{RFF} and $3f_{RFF}$, which indicate the presence of a bearing roller fault.

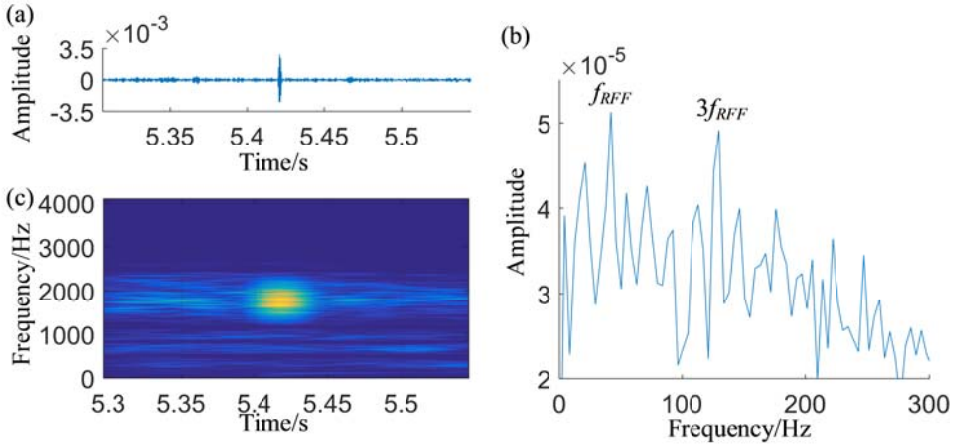

Figure 22 Fault feature signal extracted by SK - Case 2 (a) time domain waveform (b) Hilbert envelope spectrum (c) time-frequency representation of the fault feature signal

Conclusion

In this paper, a novel method based on a combination of the MSCPP method, the application of a series of VDFs and a new motion parameter estimation method is proposed and demonstrated to be suitable for the removal of the Doppler Effect from wayside acoustic signals. The effectiveness of the proposed method has successfully been verified through testing with a known simulated signal and through two case studies. The MSCPP component of the proposed method has been shown to be able to extract IFs corresponding to relevant harmonic components. VDFs, whose centre frequencies are chosen by fitting curves to the IFs, are then constructed and used to exclude these main harmonic components. The motion parameters of the train bearing can be estimated, using the new motion parameter estimation method, and used to generate a resampling time vector. Finally, the Doppler-free signal can be obtained by resampling the residual signal from the VDF outputs using the resampling time vector. Fault feature extraction is then demonstrated by applying the SK method to the Doppler-free signals. Computation for the approach can be undertaken using a standard laptop computer sufficiently quickly that in a deployed system it could occur between vehicle passages. The proposed method has been evaluated using both simulation and field experiments. The following conclusions are obtained through consideration of this testing:

(1) The MSCPP method is a powerful tool for the extraction of IFs. However, it is not possible to automatically select its parameters which somewhat limits its practical application. Hence, adaptive parameter selection for MSCPP is a target of further research.

(2) The new motion parameter estimation method is effective. However, the results are highly dependent on accurate IF estimation. Improved IF extraction methods should, therefore, be a target of future research.

(3) In this work, light-gate sensor was used to identify the vehicle passage and define the detection period for the target bearing. In order to decrease the cost and improve practicality, a method which can be used to extract several IFs simultaneously should be researched.

Acknowledgements

This study was supported by the China Scholarship Council and the Guangzhou Science and Technology Plan (Ref. 201704030048), and makes use of data recorded

during previous studies sponsored by Hitachi Rail Europe. The authors would like to express their gratitude to Rail Alliance and Motorail Logistics for providing access to their test facilities.

Reference

1. Dybała, J. and S. Radkowski, *Reduction of Doppler effect for the needs of wayside condition monitoring system of railway vehicles.* Mechanical Systems and Signal Processing, 2013. 38(1): p. 125-136.
2. He, Q., et al., *Wayside acoustic diagnosis of defective train bearings based on signal resampling and information enhancement.* Journal of Sound and Vibration, 2013. 332(21): p. 5635-5649.
3. Wang, J., Q. He, and F. Kong, *A new synthetic detection technique for trackside acoustic identification of railroad roller bearing defects.* Applied Acoustics, 2014. 85: p. 69-81.
4. Entezami, M., et al. *Acoustic analysis techniques for condition monitoring of roller bearings*. in *Railway Condition Monitoring (RCM 2014), 6th IET Conference on*. 2014. IET.
5. Liu, F., et al., *Doppler effect reduction scheme via acceleration-based Dopplerlet transform and resampling method for the wayside acoustic defective bearing detector system.* Proceedings of the Institution of Mechanical Engineers, Part C: Journal of Mechanical Engineering Science, 2014. 228(18): p. 3356-3373.
6. Wang, C., et al., *Wayside acoustic defective bearing detection based on improved Dopplerlet transform and Doppler transient matching.* Applied Acoustics, 2016. 101: p. 141-155.
7. Shen, C., et al., *A parameterized Doppler distorted matching model for periodic fault identification in locomotive bearing.* Proceedings of the Institution of Mechanical Engineers, Part C: Journal of Mechanical Engineering Science, 2015: p. 0954406215616416.
8. Liu, Y., et al., *Wayside Bearing Fault Diagnosis Based on Envelope Analysis Paved with Time-Domain Interpolation Resampling and Weighted-Correlation-Coefficient-Guided Stochastic Resonance.* Shock and Vibration, 2017. 2017.
9. Liu, F., et al., *Doppler effect reduction based on time-domain interpolation resampling for wayside acoustic defective bearing detector system.* Mechanical Systems and Signal Processing, 2014. 46(2): p. 253-271.
10. Wang, C., et al., *De-noising of wayside acoustic signal from train bearings based on variable digital filtering.* Applied Acoustics, 2014. 83: p. 127-140.
11. Wang, C., et al., *Doppler Effect removal based on instantaneous frequency estimation and time domain re-sampling for wayside acoustic defective bearing detector system.* Measurement, 2014. 50: p. 346-355.
12. Timlelt，Hakima, Y. Remram, and A. Belouchrani, *Closed-form solution to motion parameter estimation of an acoustic source exploiting Doppler effect.* Digital Signal Processing, 2017.
13. Candes, E.J., P.R. Charlton, and H. Helgason, *Detecting highly oscillatory signals by chirplet path pursuit.* Applied and Computational Harmonic Analysis, 2008. 24(1): p. 14-40.

14. Qian, S. and D. Chen, *Joint time-frequency analysis.* IEEE Signal Processing Magazine, 1999. 16(2): p. 52-67.
15. Peng, F., D. Yu, and J. Luo, *Sparse signal decomposition method based on multi-scale chirplet and its application to the fault diagnosis of gearboxes.* Mechanical Systems and Signal Processing, 2011. 25(2): p. 549-557.
16. McClellan, J.H., R.W. Schafer, and M.A. Yoder, *Signal processing first*. 2003: Pearson/Prentice Hall.
17. Gustafsson, F., *Determining the initial states in forward-backward filtering.* IEEE Transactions on Signal Processing, 1996. 44(4): p. 988-992.
18. Chung, S. and R. Kennedy, *Forward-backward non-linear filtering technique for extracting small biological signals from noise.* Journal of neuroscience methods, 1991. 40(1): p. 71-86.
19. Dobeck, G.J. *Image normalization using the serpentine forward-backward filter: application to high-resolution sonar imagery and its impact on mine detection and classification*. in *Defense and Security*. 2005. International Society for Optics and Photonics.
20. Wu, C., et al., *Gearbox fault diagnosis using adaptive zero phase time-varying filter based on multi-scale chirplet sparse signal decomposition.* Chinese Journal of Mechanical Engineering, 2013. 26(4): p. 831-837.
21. Cheng, J., et al., *Application of frequency family separation method based upon EMD and local Hilbert energy spectrum method to gear fault diagnosis.* Mechanism and Machine Theory, 2008. 43(6): p. 712-723.
22. Morse, P.M. and K.U. Ingard, *Theoretical acoustics*. 1968: Princeton university press.
23. Zhang, Z., et al., *Enhanced fault diagnosis of roller bearing elements using a combination of empirical mode decomposition and minimum entropy deconvolution.* Proceedings of the Institution of Mechanical Engineers, Part C: Journal of Mechanical Engineering Science, 2017. 231(4): p. 655-671.
24. Ou, L., D. Yu, and H. Yang, *A new rolling bearing fault diagnosis method based on GFT impulse component extraction.* Mechanical Systems and Signal Processing, 2016. 81: p. 162-182.